Macromolecular Rapid Communications
www.mrc-journal.de

Supramolecular "Step Polymerization" of Preassembled Micelles: A Study of "Polymerization" Kinetics

Chaoying Yang, Xiaodong Ma, Jiaping Lin, Liquan Wang, Yingqing Lu, Liangshun Zhang,* Chunhua Cai, and Liang Gao*

In nature, sophisticated functional materials are created through hierarchical self-assembly of nanoscale motifs, which has inspired the fabrication of man-made materials with complex architectures for a variety of applications. Herein, a kinetic study on the self-assembly of spindle-like micelles preassembled from polypeptide graft copolymers is reported. The addition of dimethylformamide and, subsequently, a selective solvent (water) can generate a "reactive point" at both ends of the spindles as a result of the existence of structural defects, which induces the "polymerization" of the spindles into nanowires. Experimental results combined with dissipative particle dynamics simulations show that the polymerization of the micellar subunits follows a step-growth polymerization mechanism with a second-order reaction characteristic. The assembly rate of the micelles is dependent on the subunit concentration and on the activity of the reactive points. The present work reveals a law governing the self-assembly kinetics of micelles with structural defects and opens the door for the construction of hierarchical structures with a controllable size through supramolecular step polymerization.

1. Introduction

Hierarchical architectures created via the self-assembly of nanoscale building blocks are ubiquitous in biological systems. In the case of man-made self-assembly, this natural phenomenon has inspired the fabrication of complex functional hierarchies, with the aim of developing bottom-up approaches for elegant structuring of advanced materials.[1–8] Among the self-assembled hierarchies, 1D superstructures are of special interests because of their potential applications as vehicles for drug delivery,[9,10] rheology modifiers,[11] and models for the mechanistic understanding of protein fiber formation,[12,13] such as the formation of actin fibers. Achieving precise control of the nanostructure is of great significance to improve the performance of 1D structured materials.

Dr. C. Yang, Dr. X. Ma, Prof. J. Lin, Prof. L. Wang, Dr. Y. Lu, Prof. L. Zhang, Prof. C. Cai, Dr. L. Gao
Shanghai Key Laboratory of Advanced Polymeric Materials
State Key Laboratory of Bioreactor Engineering
Key Laboratory for Ultrafine Materials of Ministry of Education
School of Materials Science and Engineering
East China University of Science and Technology
Shanghai 200237, China
E-mail: jlin@ecust.edu.cn; zhangls@ecust.edu.cn

DOI: 10.1002/marc.201700701

Recently, using anisotropic preassemblies as subunits for 1D self-assembly has emerged as an efficient route to prepare 1D nanostructures.[14–20] Through noncovalent interactions or chemical reactions, the anisotropic subunits created from block/graft copolymers can act as the monomer unit and "polymerize" themselves into a supramolecular polymer. For example, Liu and co-workers prepared two types of block copolymer nanotubes with carboxyl or amino terminal groups.[14,15] The terminal groups then reacted via amidization to join the nanotubes head to tail, which resulted in the formation of a dimer or trimer composed of nanotubes. Müller and co-workers prepared various, well-defined multicompartment micelles (MCMs) with precisely tunable patchiness.[16,17] Under suitable conditions, the step polymerization of anisotropic MCMs into mesoscale supramolecular polymers can be triggered. Sohn and co-workers demonstrated supramolecular polymer chains of diblock copolymer micelles.[18] By increasing the polarity of the solvent, the preformed spherical micelles were converted to anisotropic subunits and polymerized into linear supramolecular chains. We have reported that anisotropic spindle-like micelles, self-assembled from poly(γ-benzyl-L-glutamate)-*graft*-poly(ethylene glycol) (PBLG-*g*-PEG), can act as ideal preassembled subunits to construct 1D materials with hierarchical structures.[19] Upon the addition of dimethylformamide (DMF) and dialysis against water, the structural defects can serve as "reactive points" that subsequently drive the connection of the anisotropic micelles in an end-to-end manner to form a hierarchical nanowire structure.

However, despite the advances in the design and construction of 1D superstructures, some important issues remain unsolved. For example, thus far, most studies on 1D assembly of micellar subunits have focused on the thermodynamics-driven morphological transition of the self-assemblies; no quantitative approach has been successfully applied to the kinetics of 1D growth. This lack of a quantitative approach represents a challenge for understanding the self-assembly of micellar subunits. The quantitative approach for studying the kinetics has been applied to only the self-assembly of inorganic nanoparticles, which are distinct from the micelle systems in terms of the size and structure rigidity of subunit.[21–23] Understanding

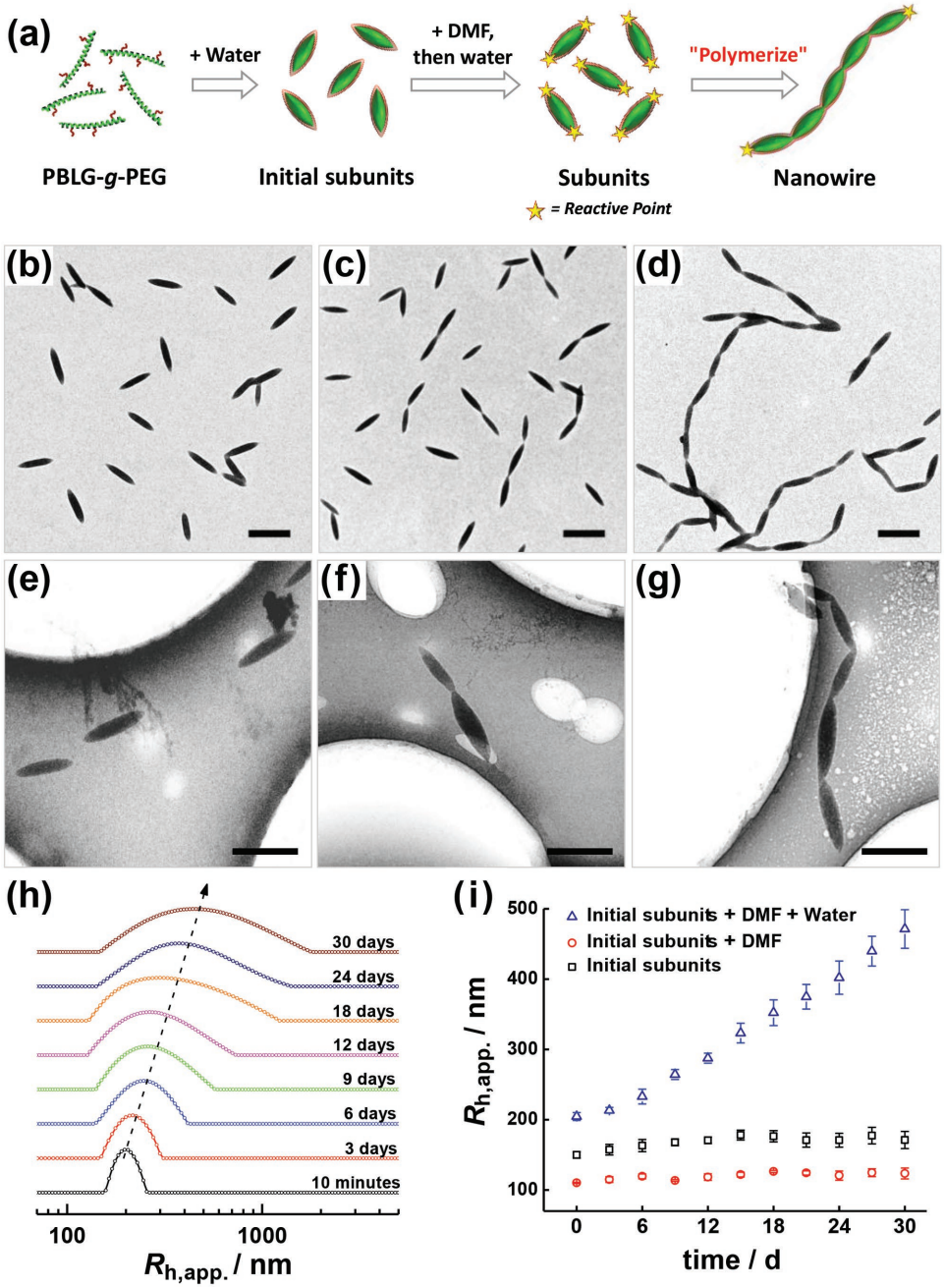

Figure 1. Self-assembly of spindle-like subunits into nanowires. a) Illustration of the self-assembly processes of nanowires from spindle-like subunits. b–d) TEM and e–g) cryo-TEM images of the aggregates self-assembled from subunits with various self-assembly times (t): b,e) 10 min, c,f) 6 d, and d,g) 30 d. Scale bar: 500 nm. h) Time evolution of $R_{h,app.}$ distribution function of subunits in solution. The arrows are included only to guide the eye. i) Plots of the apparent hydrodynamic radius, $R_{h,app.}$, versus t for the initial subunit solution (black squares), the subunit solution where only DMF was added (red circles), and the subunit solution where both DMF and water were added (blue triangles). The $R_{h,app.}$ was measured at a scattering angle of 90°.

the "polymerization" kinetics of preassembled micelles and the statistics of the self-assembly of 1D structures can enable the quantitative prediction of structural features and the controllable fabrication of 1D materials. Additionally, the majority of existing 1D assembly methods are applicable to only certain types of polymers. Developing a general self-assembly method has both theoretical and practical significance and can offer new and diverse opportunities for further applications.

In our previous work, we reported on the 1D supramolecular polymerization of PBLG-*g*-PEG anisotropic preassemblies driven by structural defects of the preassemblies.[19] Herein, to address abovementioned challenges such as controllability of the 1D self-assembly process, we improved the stepwise experimental method by replacing the dialysis process with the addition of water (**Figure 1**a). The length of the formed nanowires can be precisely manipulated via the amount of DMF

and water added. This new experimental method enabled us to study the kinetics of the 1D growth of anisotropic preassemblies, which helped to reveal the mechanism of 1D supramolecular polymerization. In addition, we conducted the theoretical simulation to deepen the understanding on the kinetics of the supramolecular polymerization. To our best knowledge, this is the first example regarding the quantitative analysis of the 1D assembly kinetics of polymer micelles, which can help not only the development of new theories on the self-assembly of micellar subunits, but also the controllable fabrication of 1D hierarchical nanostructures in the future.

2. Results and Discussion

2.1. Kinetics of Self-Assembly of Preassembled Micelles into Nanowires

In a typical experiment, initial spindle-like micelles (initial subunits) were prepared by adding selective solvents (water, 1.0 mL) to 4.0 mL of a PBLG-*g*-PEG/tetrahydrofuran (THF)/DMF initial solution (THF/DMF (2/2, v/v) with an initial polymer concentration of 0.6 g L^{-1}). In the second step, 3.0 mL of DMF was pipetted into the initial subunit solution to create reactive points at each end of the spindle-like subunits where the ends are not well covered by the PEG chains (the DMF content was 62.5 vol%); 6.0 mL of water was then added to "activate" the spindle-like subunits (water content was 50.0 vol%). As a consequence of the structural defects at both ends of the spindle, a higher energy can be generated when DMF and water are added.[19] This higher energy endows the reactive points at the ends with sufficient activity to induce the self-assembly of the subunits (the existence of the structural defects at the spindle ends is confirmed by the control experiments and simulations. See details in Sections S4.1 and S5.4 of the Supporting information). To characterize the morphology change over the self-assembly time using transmission electron microscopy (TEM) and scanning electron microscopy (SEM), at intervals of 6 d, we pipetted 0.5 mL of the sample solution into a large amount of water to freeze the morphologies.[24,25] Experimental details are provided in Section S1 of the Supporting Information.

Figure 1b–d shows TEM images of the aggregates self-assembled from the activated subunits at different assembly times (t). As evident in the figure, the sample at 10 min displays separated spindle-like micelles with a mean length of ≈400 nm (Figure 1b). With increasing assembly time, the nanowire structures were formed through end-to-end connection of the subunits and the number of subunits in the nanowires gradually increased (Figure 1c,d). The corresponding cryo-TEM images, as shown in Figure 1e–g, reveals the same morphology change as conventional TEM. Thus, a possible drying effect on the formation of the nanowire structures can be ruled out. This time-dependent connection of spindles was also examined by SEM and similar results are obtained (Figure S2, Supporting Information). To monitor the self-assembly process of the activated subunits in situ, we measured the apparent hydrodynamic radius ($R_{h,app.}$) of the subunits in solution using dynamic light scattering (DLS) technology (Figure S3, Supporting Information). Figure 1h shows the distribution of the $R_{h,app.}$ of the subunits in solution at different assembly times. The results revealed that the peak maximum shifts gradually toward a higher $R_{h,app.}$ over time, which suggests a progressive connection of the subunits. The distribution of the $R_{h,app.}$ becomes broader as well, which indicates that the size of the nanowires (associated with the number of repeat subunits) exhibits polydispersity. The corresponding plots of $R_{h,app.}$ versus time are presented in Figure 1i (blue up-triangles), and the gradual increase of $R_{h,app.}$ confirms the growth of the nanowires. The DLS results are in good agreement with the morphology observations. Since the DLS characterization was not affected by the drying process of solution, the above result further proves that the hierarchical nanowires were formed in the solution as a result of the connection of the subunits. To understand the roles of the DMF and water that were added during the self-assembly process, we conducted a control experiment of DLS measurements for the initial subunit solution and a subunit solution with only DMF added. The variation of $R_{h,app.}$ of these two solutions as a function of time is also presented in Figure 1i. As evident in this figure, the $R_{h,app.}$ values of both solutions were almost unchanged over time, which suggests that no progressive changes occur in the morphology. This control study further confirmed that upon the addition of DMF and water, the spindle-like subunits can be "activated." The reactive points with a higher energy, which are generated by adding water, enable the polymerization of the preassembled micelles.

To gain insights into the formation mechanism of the nanowire, we further analyzed the kinetic data using the method adopted in traditional polymerization. For different self-assembly times, t, the distribution of the degrees of "polymerization" of the nanowires (equivalent to the distribution of the nanowires with various numbers of subunits) can be described by the number fraction, f_X, of the nanowires with degrees of "polymerization" (X). We obtained this value by collecting SEM images of more than 500 micelles and analyzing the images using the Image-Pro Plus software (Section S2, Supporting Information). **Figure 2**a shows the f_X of the nanowires with various X. As shown in Figure 2a, the number fraction of the unreacted spindle ($f_{X=1}$) decreases with increasing time, which means that the number fraction of spindles joining in the polymerization gradually increases with time. For example, $f_{X=1}$ was ≈0.95 at t = 10 min and 0.27 at t = 30 d. Interestingly, f_X exhibits an exponential decay with X at each assembly time, and the f_X data can be fitted by the relationship $f_X = (1-p)p^{X-1}$, where p represents the extent of polymerization.[26] A representative theoretical fitting curve is given by a blue dashed line for the samples "polymerized" for 18 d (Figure 2a). Other results were omitted for clarity (the other results are available in Figure S4 of the Supporting Information). The agreement between the experimental data and theoretical prediction implies that the connection of the subunits can follow a step-by-step manner, which is a rule for the step polymerization of monomers.

We further examined the effect of the initial concentration of subunits (C_{sub}) on the growth of the nanowires. Here, the value of C_{sub} was initially designated as C_0. To obtain a range of C_{sub}, we diluted the subunits of C_0 into $0.8C_0$, $0.6C_0$, $0.4C_0$, $0.2C_0$, and $0.1C_0$. All of the samples had the same solvent

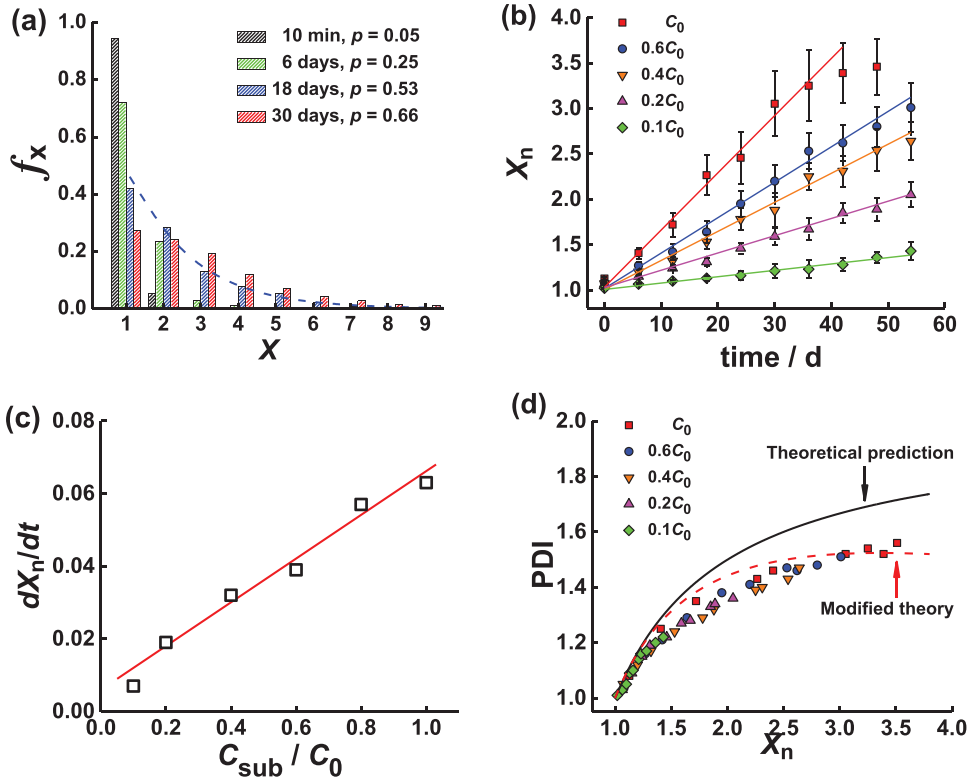

Figure 2. "Polymerization" of the spindle-like subunits. a) The number fraction, f_X, of the nanowires as a function of the degree of "polymerization" X at various assembly times. The blue dashed line is the theoretical number fraction, f_X, of the nanowires with X ($f_X = (1-p)p^{X-1}$, $p = 0.53$). "Polymerization" of the subunits at various concentration of subunits C_{sub}: C_0 (red squares), $0.6C_0$ (blue circles), $0.4C_0$ (orange down-triangles), $0.2C_0$ (magenta up-triangles), and $0.1C_0$ (bright-green diamonds). b) Variation in the number-average degree of "polymerization", X_n, with time, t. c) Dependence of the chain growth rate on C_{sub}. d) Variation in the PDI of the nanowires with X_n. The black solid line shows the theoretical prediction of $PDI_{theory} = 2 - 1/X_n$, and the red dashed line represents the fitting curve according to the modified theory.

composition (i.e., THF:DMF:water = 2:5:7 v/v/v). In addition, to characterize the evolution of the average aggregate size and the size distribution of the nanowire aggregates, we adopted two parameters defined in our previous work.[19] One is the number-average degree of "polymerized" of the nanowires (X_n), which describes the number-average length of the nanowires; the other is the polydispersity index (PDI), which characterizes the size distribution. Details of the definitions and measurements are presented in Section S2 of the Supporting Information.

For the concentration range studied, X_n as a function of t is plotted in Figure 2b. The value of X_n increases linearly with time, which gives chain growth rates of dX_n/dt for each C_{sub}. The growth kinetics of the nanowire was also examined by DLS, and a similar dependence on the concentration is shown (Figure S5, Supporting Information). The dX_n/dt was found to be linearly proportional to the C_{sub} (Figure 2c). The linear increase of X_n with time and the linearly proportional relationship between dX_n/dt and C_{sub} are two characteristics of the second-order reaction kinetics of the step-growth polymerization of monomers.[21,26,27] Therefore, the growth of nanowires generally follows the rules of step polymerization. Similar to the rule in step polymerization, the variation of X_n of the nanowires can be fit by the relationship $X_n = C_{sub}kt + 1$, where k is the assembly rate constant with a value of $0.06 \cdot (C_0^{-1}\ d^{-1})$ and d represents the time unit of day.

Furthermore, for all the values of C_{sub}, the PDI as a function of X_n is plotted in Figure 2d. The PDI increases with X_n and approaches a value of 1.5 for the whole assembly time. Compared to the theoretical PDI prediction ($PDI_{theory} = 2 - 1/X_n$) in step polymerization,[26] the PDI in the experiment was smaller, which suggests that the growth of the nanowires does not fully satisfy the rules of the step polymerization of bifunctional monomers with equal end-group reactivity. With respect to the polymeric subunits, their structures usually have variations that produce structural differences in the endcaps, which leads to variations in the activities. Thus, we observed a deviation from the theoretical line at higher values of X_n. To verify this assumption, we modified the theory by introducing a parameter α, which is defined as the ratio of the activities of the two reactive points of a subunit. In this modification, we simply assumed that the structures of all the subunits are the same, but the two ends possess different reactivities (see Section S3 of the Supporting Information). The best-fitting α value was 1.66, and the fitting improved significantly (see red dashed line in Figure 2d).

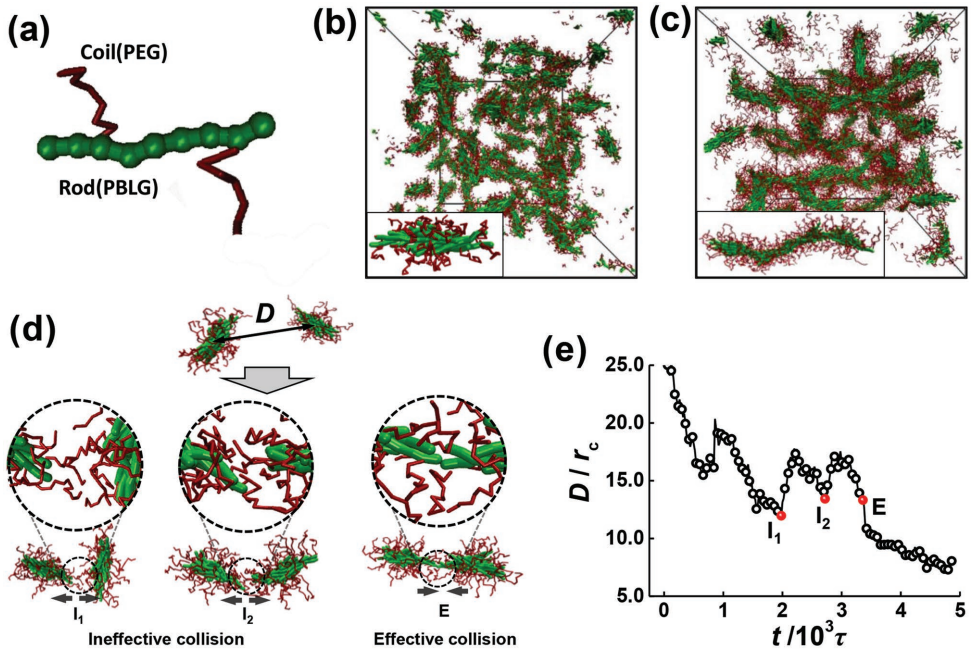

Figure 3. DPD simulation of the supramolecular "step polymerization" process. a) DPD model of a rod-*g*-coil graft copolymer. Simulation snapshots of the aggregates self-assembled from spindle-like subunits at different simulation times: b) 0τ, c) $160 \times 10^3\tau$. Detailed assembly mechanism of the subunits in solution. d) Collision manners in the course of the assembling process of subunits in solution. The dashed cycles enlarge the contact position of the subunits. e) Temporal variation of the center distance, *D*, between the activated subunits in a representative assembling process. The red dots mark the different collisions in panel (d).

2.2. Theoretical Simulation of the Supramolecular "Step Polymerization" Process

To complement the experimental studies, we applied a coarse-grained simulation method referred as dissipative particle dynamics (DPD) to explore the kinetics of the hierarchical self-assembly process.[28,29] In the DPD method, the pairwise interactions between *i* and *j* components are described by the repulsion parameter a_{ij}, which is linearly related to Flory–Huggins interaction parameter χ_{ij}.[30–32] The rigid PBLG backbones, flexible PEG side chains, and solvent molecules were coarse-grained into the **R**, **C**, and **S** beads, respectively (**Figure 3**a). At the initial settings of interaction parameters of $a_{RC} = 40.0$, $a_{RS} = 50.0$, and $a_{CS} = 25.0$, the modeled chains self-assembled into spindle-like micelles (Figure 3b). As detailedly shown in inset, the rigid backbones in the micelles align along the long axis in a manner similar to nematic liquid crystals and a defect is generated in each end of the micelle due to the imperfect coverage of the flexible blocks. To model a change in the solvent environment, i.e., the addition of PBLG-selective DMF to the solution of micelles, the interaction parameter between the **R** and **S** beads was changed from $a_{RS} = 50.0$ to $a_{RS} = 40.0$. Under this condition, the rigid core swells, which results in more exposure of the rigid backbones to the solvents in both ends. The subsequent addition of water is modeled by the changes of a_{RS} from 40.0 to 100.0 because of the decrease in solubility of the solvents to PBLG, and a_{CS} from 25.0 to 20.0 owing to the hydrogen bonds between PEG and water. Additionally, because the molecular exchange among the spindle-like subunits during the subsequent self-assembly was hindered, we fixed the cores of the subunits as rigid bodies. Under the variation of solvent condition, the subunits connected spontaneously into nanowires via end-to-end manner, and the length of the nanowires gradually increased with time. Compared to the nanowires in the experiments, the nanowires formed by the simulations possess the similar structures in which the **R** blocks constitute a rigid core and the **C** blocks protrude outside to maintain stability (Figure 3c). From both the simulations and experiments, we deduced that the structural defect is essential for producing the "reactive points" for the supramolecular "step polymerization." This process can be generalized to other micellar units as long as "reactive points" can be produced from the existing structural defects by changing the environmental conditions (see Section S4.8 of the Supporting Information for details).

One of the advantages of DPD simulations is the ability to illuminate the assembly mechanism. Figure 3d shows the representative snapshots of the assembling structures of two activated subunits. In the initially configuration, these two subunits have a long distance. The Brownian motion of the subunits in solution induces the random collisions to each other. Since the reactive points are imperfectly covered by the mutually repulsive **C** blocks, the different collision manners in the course of assembly could occur. When the subunits collide from the side (snapshot I_1), or from the end deviating from the long axis (snapshot I_2), an ineffective collision occurs. However, when the subunits collide from the end along the long axis (snapshot E), an effective collision occurs, which leads to the successful bonding of the subunits. Figure 3e presents the temporal evolution of the center distance, *D*, between the subunits during a representative assembling process, and the red dots mark the

different collisions shown in Figure 3d. The subunits approach each other via Brownian motion, as shown by the decrease of D with time. The subunits are pushed away after the side collision (I_1) and the end collision deviating the axis (I_2), as reflected by the increase of the center distance D after the collisions. When the effective collision occurs, the subunits connect via the bonding of the rigid core, which is reflected by the quick decrease in D after the point marked by E. We also calculated the fraction of effective collisions, f, which is defined as the ratio of the number of effective collisions to the number of total collisions. The value of f was 0.046, which means an average of 22 collisions is required to generate one effective collision (see Section S5.3 of the Supporting Information for details). This assembly mechanism of the subunits is analogous to molecular polymerization in which only an effective collision leads to bonding of the monomers; consequently, the growth kinetics of the nanowires follow the kinetics of a reaction-controlled, step-growth polymerization.[26,27]

Simultaneously, we studied the growth kinetics of the nanowires via the DPD simulations. As shown in **Figure 4**a, in agreement with the experimental findings, the number fraction of the unreacted spindle ($f_{X=1}$) decreases with time; in addition, at each time f_X decays with X following the relationship $f_X = (1-p)p^{X-1}$. To examine the effects of initial concentration C_{sub} of subunits on the number-average degree of "polymerization" (X_n), we first set the initial concentration C_{sub} as $C_0 = 130/(VN_A)$, where V is the volume of simulation box and N_A is the Avogadro's number, and subsequently changed C_{sub} as C_0, $0.8C_0$, $0.6C_0$, $0.4C_0$, and $0.2C_0$ respectively. In the range of $0.2C_0 \le C_{sub} \le C_0$, the values of X_n linearly increase with increasing assembly time, t (Figure 4b). As shown in Figure 4c, the rate of the chain growth, dX_n/dt, increases with C_{sub} in a linear trend, and the slope of the line gives the assembly rate constant k with a value of $1.5 \times 10^{-7} V N_A/\tau$. These features are characteristics of second-order step-growth polymerization, which is in agreement with the experimental observations. Additionally, the PDI for the different initial concentrations of the subunits increases with X_n (Figure 4d), which is in agreement with the feature of step-growth polymerization. Note that the PDI in the simulations is also smaller than the theoretical prediction value because of the deviation of the activities of the subunit ends from equality. By replacing the original theoretical equation with the modified one, the data fitting can be improved, as indicated by the red dashed line in Figure 4d.

2.3. Influence of Reactivity of the Preassembled Micelles

The aforementioned results reveal that the emergence of reactive points play a critical role in the appearance of

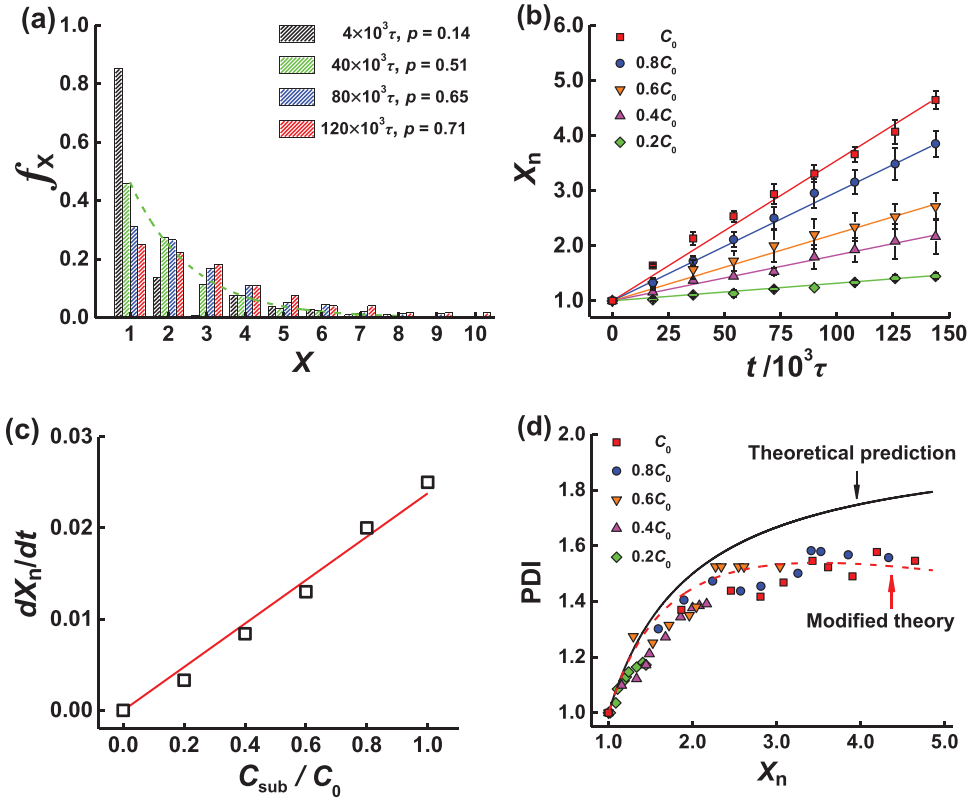

Figure 4. "Polymerization" of the spindle-like subunits in the simulations. a) Number fraction, f_X, of the nanowires as a function of the degree of "polymerization" X at various assembly times. The green dashed line is the theoretical number fraction, f_X, of the nanowires with X ($f_X = (1-p)p^{X-1}$, $p = 0.51$). "Polymerization" of the subunits at various initial subunit concentrations, C_{sub}: C_0 (red squares), $0.8C_0$ (blue circles), $0.6C_0$ (orange down-triangles), $0.4C_0$ (magenta up-triangles), and $0.2C_0$ (bright-green diamonds), where $C_0 = 130/VN_A$. b) Variation in the number-average degree of "polymerization", X_n, with simulation time. c) Dependence of the chain growth rate on C_{sub}. d) Variation in the PDI of the nanowires with X_n. The black solid line shows the theoretical prediction of $PDI_{theory} = 2 - 1/X_n$, and the red dashed line represents the fitting curve according to the modified theory.

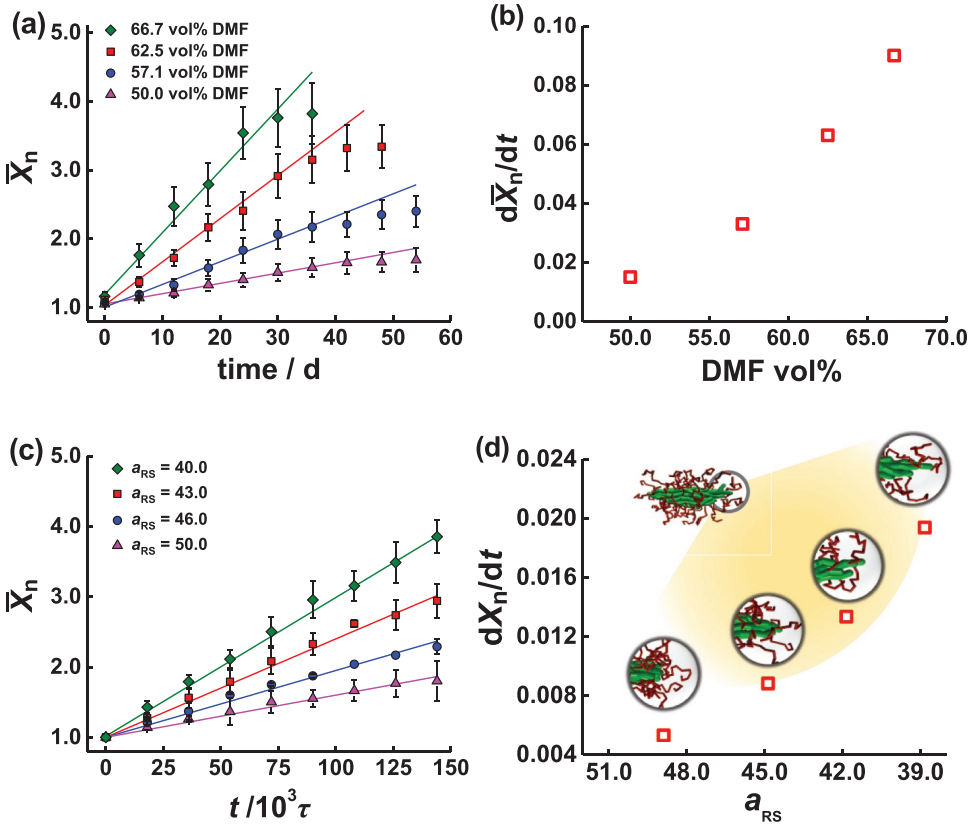

Figure 5. Effect of DMF content on the "polymerization" of the subunits. a) Variation in X_n with assembly time at various DMF contents. b) Dependence of the chain growth rate on DMF content at a constant C_{sub}. c) Variation in X_n with simulation time at various a_{RS}. d) Dependence of the chain growth rate on a_{RS} at a constant C_{sub} in the DPD simulations. The insets illustrate the structure of the spindle-like subunits in simulations for a_{RS} = 50.0, 46.0, 43.0, and 40.0.

polymerization-like self-assembly processes. The activity of the reactive points may affect the supramolecular polymerization process, which is similar to the manner in which functional-group activity affects the step polymerization of monomers. To examine this effect, we varied the amount of DMF added to the initial subunit solution. This approach was used because the exposure of the hydrophobic PBLG segments in the subunit ends can be manipulated via the amount of DMF present. The effect of the DMF content on the activity of the reactive points was revealed by the kinetic data presented in **Figure 5**. Figure 5a shows that at the different DMF contents studied, the value of X_n increased linearly with t, which follows the relationship $X_n = C_{sub}kt + 1$. Moreover, the value of X_n increased faster when greater amounts of DMF were added, as revealed by the slopes of the relationship $X_n \approx t$ (the corresponding DLS results show some tendency, and they are given in Figure S6 of the Supporting Information). The rate of the chain growth at various DMF contents is defined by the slopes, dX_n/dt. As shown in Figure 5b, the value of dX_n/dt increases with increasing DMF content, which indicates that a greater DMF content accelerates the growth of nanowires because more PBLG chains are exposed to the solvent.

The effect of the DMF content on the growth rate of the nanowires was also examined via the DPD simulations. To model the increased content of PBLG-selective DMF, a solution of spindle-like micelles formed in the initial interaction parameters was simulated with a series of interaction parameters a_{RS} = 50.0, 46.0, 43.0, and 40.0. In the subsequent self-assembly of the subunits, the interaction parameters were changed to a_{RC} = 40.0, a_{RS} = 100.0, and a_{CS} = 20.0, which corresponds to the addition of water to the solution. As shown in Figure 5c, the nanowire growth kinetics for the subunits formed at various a_{RS} follow a linear $X_n \approx t$ relationship. The decrease of a_{RS} (increase in the DMF content) leads to an increase in the rates of the chain growth dX_n/dt (Figure 5d), in good agreement with the experimental findings. To clarify the effect of the DMF content, we compared the structures of the spindle-like subunits formed at different a_{RS}. As illustrated in the insets of Figure 5d, a decrease in a_{RS} results in swelling of the rigid cores with more solvophobic PBLG backbones protruding from the ends of the subunits and exposing themselves to the solvent. We also computed the fraction of effective collisions, f, for the various DMF contents. The value of f increases with increasing DMF contents. This is obviously the consequence of the swelling of rigid cores. Moreover, a linear relationship between the growth rate, dX_n/dt, and f was observed (Figure S8b, Supporting Information). This is in good agreement with the classical collision theory in chemical reaction kinetics.[33]

Our experimental and theoretical findings show that the self-assembly of micellar subunits into 1D nanowires resembles many aspects of molecular step-growth polymerization, such as the end-to-end connection of building units, the Flory's

equations of kinetics, and the linear configuration of products. Despite the physical analogies to the molecular step-growth polymerization, there exist some distinctive characteristics in step-growth polymerization of the micellar subunits. Specifically, the assembly rate constant, k, ($\approx 10^2$ M^{-1} s^{-1}, the estimation of k is shown in Section S4.7 of the Supporting Information) is considerably larger than that of molecular step-growth polymerization (typically in the range of $\approx 10^{-3}$–10^{-5} $M^{-1} \cdot s^{-1}$), since the molecules are chemically bonded and their connection requires higher activation energy.[26,27] The k value is also found to be smaller than that of the assembly of inorganic nanoparticles ($\approx 10^4$ M^{-1} s^{-1}), because the inorganic nanoparticles possess higher mobility in solution resulting from their smaller size (≈50 nm in length) than that of the micellar subunits (≈400 nm in length).[21,34] Our nontrivial finding suggests that the self-assembly of micellar subunits can be used effectively to mimic molecular polymerization with practical time scales. In addition, in contrast to the molecular rate constant which is dependent on the activation energy, the assembly rate constant of nanowires is primarily determined by the exposure of reactive points in the ends of the micellar subunits, which provides new heuristic guidelines for the fabrication of 1D polymer-like nanowires.

3. Conclusions

In summary, we reported the first example, to our knowledge, of the kinetics of supramolecular "step polymerization" of micellar subunits. Such "polymerization" displays the characteristics of a second-order reaction, and the assembly rate is dependent on the subunit concentration and its reactivity. The knowledge obtained from this study is useful for realizing controllable syntheses of 1D superstructures and represents a significant step forward in hierarchical self-assembly. The combined experimental and theoretical simulation studies greatly deepen our understanding of the mechanism of the supramolecular polymerization. The existence of structural defects in the preassemblies is essential for the polymerization. As long as the structural defects exist in the micelles, the "reaction point," which has a higher energy, can be generated through changes in the solvent conditions. This control of the reaction point enables the "polymerization" of the preassembled micelles. Using this principle, we can design and prepare sophisticated materials taking use of the defects on self-assemblies, which may have potential applications in biomedical fields.

4. Experimental Section

Polymer Synthesis: PBLG was obtained through the ring-opening polymerization of γ-benzyl-L-glutamate-*N*-carboxyanhydride initiated by triethylamine with 1,4-dioxane as the solvent.[19,25,35,36] PBLG-*g*-PEG was prepared via the ester exchange reaction of PBLG with mPEG-OH.[19,37] At the end of the two polymerizations, the reaction mixture was precipitated into a large volume of anhydrous methanol. The product was purified twice via repeated precipitation from a chloroform solution into a large volume of anhydrous methanol and dried under vacuum. Details of the polymer synthesis are shown in Section S1.1 of the Supporting Information.

Preparation of the Assemblies: Polymer assemblies were prepared using the following procedure. First, PBLG-*g*-PEG graft copolymers were dissolved in THF/DMF (1/1, v/v) mixed solvents via stirring at room temperature for 2 d to obtain the stock solutions. Typically, 1.0 mL of deionized water was added to 4.0 mL of the PBLG-*g*-PEG initial solution (polymer concentration of 0.6 g L^{-1}) with vigorous stirring to form subunits (initial subunit solution). Then, 3.0 mL of DMF was pipetted into the initial subunit solution (DMF content of 62.5 vol%). Subsequently, 6.0 mL of water was quickly added to "activate" the subunits and induce the self-assembly of the subunits (subunit solution, water content of 50.0 vol%). At intervals of 6 d, we pipetted 0.5 mL of the subunit solution into a large amount of water to freeze the morphologies. The sample solution was dialyzed against deionized water for 3 d to ensure that all organic solvents were removed. To investigate the effect of the concentration of the subunits (C_{sub}) on the self-assembly, we diluted the subunit solutions into various volumes using the same solvent composition (i.e., THF:DMF:water = 2:5:7 v/v/v). For studies on the effect of the added DMF content on the self-assembly, various volumes of DMF were added to the initial subunit solution and the added water content was fixed at 50.0 vol% for all samples. Note that in the aforementioned experiments where the effect of DMF was studied, the concentration of the subunits (C_{sub}) was kept the same for the same set of samples and the influence of C_{sub} on the growth of the nanowires could be ruled out.

Characterization of the Assemblies: The morphologies were characterized using TEM (JEM-2100F, JEOL, 200 kV), SEM (S4800, Hitachi, 15 kV), and cryo-TEM (FEI T20, 200 kV, −174 °C). The apparent hydrodynamic radius of the aggregates was measured using DLS (CGS-5022F, ALV, laser wavelength 632.8 nm). The values of f_X, p, X_n and PDI were obtained by collecting SEM images with more than 500 micelles and analyzing the images using the Image-Pro Plus software. The detailed experimental information is available in Sections S1.2–S1.6 and S2.0 of the Supporting Information.

Simulation Methods: DPD is a particle-based mesoscopic simulation technique in which a volume of several molecules or parts of molecules are represented by a coarse-grained bead.[28–32] The temporal evolution of the simulated system was achieved via integration of Newton's equation of motion, $d\mathbf{r}_i/dt = \mathbf{v}_i$ and $m_i\, d\mathbf{v}_i/dt = \mathbf{f}_i$. The total force, $\mathbf{f}_i$, acting on the i-th bead is the sum of the conservative force, $\mathbf{F}_{ij}^C$, dissipative force, $\mathbf{F}_{ij}^D$, and random force, $\mathbf{F}_{ij}^R$, i.e., $\mathbf{f}_i = \sum_{j\neq i}(\mathbf{F}_{ij}^C + \mathbf{F}_{ij}^D + \mathbf{F}_{ij}^R)$, and all the pairwise forces are truncated at a certain cutoff radius, r_c. In addition, all the conjoined beads in the grafting copolymer are bonded by a harmonic spring force given by $\mathbf{F}_{ij}^S = -C^S(r_{ij} - r_{eq})\hat{\mathbf{r}}_{ij}$, where C^S and r_{eq} denote the spring constant and equilibrium bond length, respectively. Two additional harmonic spring forces, which are $\mathbf{F}_{ij}^1$ between the first and third beads in every three neighboring beads and $\mathbf{F}_{ij}^2$ between the first and end beads of the entire rigid block, were added to the rigid blocks. An angle force, $\mathbf{F}_{ij}^\theta = -\nabla[k_\theta(\cos\theta - \cos\pi)^2]$, was also applied to the rigid blocks to constrain the bond angle near π.[38] The spring constant is $C^S = 100$, and the angle constant is $k_\theta = 20$. The equilibrium bond distances, r_{eq}, for $\mathbf{F}_{ij}^S$, $\mathbf{F}_{ij}^1$ and $\mathbf{F}_{ij}^2$ were set as 0.7, 1.4, and 5.6, respectively. Details are provided in the Section S5.1 of the Supporting Information.

All the simulations were performed in cubical boxes with edge length $60r_c$ under the periodic boundary conditions. The cutoff radius of interaction was set as $r_c = 1$. The integration step of DPD simulations was set as $\delta t = 0.04\tau$, where τ was defined as $\tau = (mr_c^2/k_BT)^{1/2}$. In the formation of spindle-like micelles from graft polymer, typical DPD simulations with 10^5 steps were performed to guarantee the equilibrium of the structures. In the subsequent assembly of the subunits, each simulation took 4×10^6 steps. Simulations from different initially random configurations with various seeds were also performed to ensure that the observations were not accidental. The detailed simulation information is available in Section S5.2 of the Supporting Information.

Supporting Information

Supporting Information is available from the Wiley Online Library or from the author.

Acknowledgements

C.Y. and X.M. contributed equally to this work. This work was supported by the National Natural Science Foundation of China (21234002, 21474029, 51573049). Supports from projects of the Shanghai municipality (16520721900, 14DZ2261205) and fundamental research funds for the central university (222201717021) are also appreciated.

Conflict of Interest

The authors declare no conflict of interest.

Keywords

kinetics, micelles, simulations, supramolecular structures

Received: October 17, 2017
Published online: December 6, 2017

[1] S. I. Stupp, V. LeBonheur, K. Walker, L. S. Li, K. E. Huggins, M. Keser, A. Amstutz, *Science* **1997**, *276*, 384.
[2] G. M. Whitesides, B. Grzybowski, *Science* **2002**, *295*, 2418.
[3] Q. Chen, S. C. Bae, S. Granick, *Nature* **2011**, *469*, 381.
[4] K. Miszta, J. de Graaf, G. Bertoni, D. Dorfs, R. Brescia, S. Marras, L. Ceseracciu, R. Cingolani, R. van Roij, M. Dijkstra, L. Manna, *Nat. Mater.* **2011**, *10*, 872.
[5] S. C. Glotzer, M. J. Solomon, *Nat. Mater.* **2007**, *6*, 557.
[6] L. J. Hill, N. Pinna, K. Char, J. Pyun, *Prog. Polym. Sci.* **2015**, *40*, 85.
[7] K. Thorkelsson, P. Bai, T. Xu, *Nano Today* **2015**, *10*, 48.
[8] N. Petzetakis, A. P. Dove, R. K. O'Reilly, *Chem. Sci.* **2011**, *2*, 955.
[9] P. Dalhaimer, A. J. Engler, R. Parthasarathy, D. E. Discher, *Biomacromolecules* **2004**, *5*, 1714.
[10] Y. Geng, P. Dalhaimer, S. Cai, R. Tsai, M. Tewari, T. Minko, D. E. Discher, *Nat. Nanotechnol.* **2007**, *2*, 249.
[11] J. M. Dean, N. E. Verghese, H. Q. Pham, F. S. Bates, *Macromolecules* **2003**, *36*, 9267.
[12] J. Qian, M. Zhang, I. Manners, M. A. Winnik, *Trends Biotechnol.* **2010**, *28*, 84.
[13] T. Ban, K. Yamaguchi, Y. Goto, *Acc. Chem. Res.* **2006**, *39*, 663.
[14] S. Stewart, G. Liu, *Angew. Chem., Int. Ed.* **2000**, *39*, 340.
[15] X. Yan, G. Liu, Z. Li, *J. Am. Chem. Soc.* **2004**, *126*, 10059.
[16] A. H. Gröschel, F. H. Schacher, H. Schmalz, O. V. Borisov, E. B. Zhulina, A. Walther, A. H. E. Müller, *Nat. Commun.* **2012**, *3*, 710.
[17] A. H. Gröschel, A. Walther, T. I. Lobling, F. H. Schacher, H. Schmalz, A. H. E. Müller, *Nature* **2013**, *503*, 247.
[18] J.-H. Kim, W. J. Kwon, B.-H. Sohn, *Chem. Commun.* **2015**, *51*, 3324.
[19] Z. Zhuang, T. Jiang, J. Lin, L. Gao, C. Yang, L. Wang, C. Cai, *Angew. Chem., Int. Ed.* **2016**, *55*, 12522.
[20] A. Wang, J. Huang, Y. Yan, *Soft Matter* **2014**, *10*, 3362.
[21] K. Liu, Z. Nie, N. Zhao, W. Li, M. Rubinstein, E. Kumacheva, *Science* **2010**, *329*, 197.
[22] K. Liu, A. Ahmed, S. Chung, K. Sugikawa, G. Wu, Z. Nie, R. Gordon, E. Kumacheva, *ACS Nano* **2013**, *7*, 5901.
[23] A. Lukach, K. Liu, H. Therien-Aubin, E. Kumacheva, *J. Am. Chem. Soc.* **2012**, *134*, 18853.
[24] L. Zhang, A. Eisenberg, *Macromolecules* **1999**, *32*, 2239.
[25] C. Cai, J. Lin, X. Zhu, S. Gong, X.-S. Wang, L. Wang, *Macromolecules* **2016**, *49*, 15.
[26] G. Odian, *Principles of Polymerization*, Wiley, New York **2004**.
[27] P. J. Flory, *Principles of Polymer Chemistry*, Cornell University Press, Ithaca, New York **1953**.
[28] P. J. Hoogerbrugge, J. M. V. A. Koelman, *Europhys. Lett.* **1992**, *19*, 155.
[29] J. M. V. A. Koelman, P. J. Hoogerbrugge, *Europhys. Lett.* **1993**, *21*, 363.
[30] T. Jiang, L. Wang, S. Lin, J. Lin, Y. Li, *Langmuir* **2011**, *27*, 6440.
[31] Y. Li, T. Jiang, S. Lin, J. Lin, C. Cai, X. Zhu, *Sci. Rep.* **2015**, *5*, 10137.
[32] Z. Xu, J. Lin, Q. Zhang, L. Wang, X. Tian, *Polym. Chem.* **2016**, *7*, 3783.
[33] K. A. Connors, *Chemical Kinetics: The Study of Reaction Rates in Solution*, John Wiley & Sons, Portland, OR, USA **1990**.
[34] L. Cademartiri, G. Guerin, K. J. M. Bishop, M. A. Winnik, G. A. Ozin, *J. Am. Chem. Soc.* **2012**, *134*, 9327.
[35] E. R. Blout, R. H. Karlson, *J. Am. Chem. Soc.* **1956**, *78*, 941.
[36] C. Cai, Y. Li, J. Lin, L. Wang, S. Lin, X.-S. Wang, T. Jiang, *Angew. Chem., Int. Ed.* **2013**, *52*, 7732.
[37] C. Cai, J. Lin, T. Chen, X. Tian, *Langmuir* **2010**, *26*, 2791.
[38] S. Lin, N. Numasawa, T. Nose, J. Lin, *Macromolecules* **2007**, *40*, 1684.